

# Quantum computation of three-wave interactions with engineered cubic couplings

Yuan Shi,\* Alessandro R. Castelli, Ilon Joseph, Vasily Geyko, Frank R. Graziani,  
 Stephen B. Libby, Jeffrey B. Parker, Yaniv J. Rosen, and Jonathan L DuBois  
*Lawrence Livermore National Laboratory, Livermore, California 94551, USA*  
 (Dated: December 22, 2024)

Quantum simulation hardware usually lacks native cubic couplings, which are essential building blocks in many physics applications. Nevertheless, we demonstrate that effective three-wave vertices can be realized on quantum computers. In particular, for the three-wave Hamiltonian of laser-plasma interactions, we show that its Hilbert space can be decomposed into a direct sum of  $D$ -dimensional subspaces. Within each subspace, physical states are readily mapped to quantum memory, and the Hamiltonian matrix becomes tridiagonal. The resultant unitary evolution is realized using two qubits on state-of-the-art quantum cloud services, which approximate the three-wave gate as products of  $\sim 20$  standard gates. This trotterization approach allows  $\sim 10$  repetitions of the three-wave gate on current quantum computers before results are corrupted by decoherence. As an alternative approach, the unitary evolution is also realized as a single gate using customized control pulses on the Quantum Design and Integration Testbed (QuDIT). Utilizing three levels of the transmon qudit, high-fidelity results are obtained for  $\sim 100$  three-wave gate repetitions. Moreover, reliable control pulses may also be synthesized cheaply using interpolation when parameters of the Hamiltonian deviate from those used in numerical optimization. Our results highlight the advantage of using customized gates in physics applications. The generalized multi-wave gates may be used to compute a large class of problems in nonlinear optics, weak turbulence, and lattice gauge theories.

The ability to couple three oscillators is crucial for both digital and analog quantum computing. In the digital approach, computation is carried out by performing a sequence of standard gate operations on qubits [1–6]. In particular, the Toffoli gate operates on three qubits, which is useful for realizing classical gates on quantum computers [7]. Even for gates that only involve two qubits, a third ancilla qubit is usually necessary for quantum error correction [8–11]. Moreover, in the analog approach, the quantum hardware is controlled to emulate problems of interest [12–22]. In many physics problems, cubic couplings in the Hamiltonian or Lagrangian constitute the lowest-order nonlinearity. On a fundamental level, three-field vertices are required to couple fermions with bosons, and mediate boson self interactions (along with four-boson terms) in nonabelian gauge theories [23]. On an applied level, three-wave couplings are responsible for parametric interactions in crystals [24], turbulence cascade in fluids [25], and cross-beam laser energy transfer in plasmas [26].

Unfortunately, quantum computing hardware does not usually provide native cubic couplings. Appreciable odd-order couplings require that the underlying physical system is strongly asymmetric under spatial inversion, which is usually absent in both the trapped-ion [27] and the superconducting [28] architectures. For example, including higher levels, the next-to-leading order effective Hamiltonian of a superconducting quantum computer, composed of Josephson-junction qubits in microwave cavities, can be approximated as [29, 30]

$$H_0 \simeq \sum_j \Omega_j a_j^\dagger a_j + \sum_{j,l} \chi_{jl} a_j^\dagger a_j a_l^\dagger a_l, \quad (1)$$

where we have used the unit  $\hbar = 1$ , and  $\Omega_j$  is the angu-

lar frequency of the  $j$ -th qubit or cavity mode. Notice that cubic coupling is absent, and the lowest-order nonlinearity is quartic, which is caused by Kerr effects with coupling strength  $\chi_{jl}$ . Given hardware Hamiltonians of this type, qubits are coupled in pairwise manner, and a question that will be answered in this letter is how odd-order couplings may be effectively generated.

As a separate question, are cubic couplings useful resources that can lead to quantum speedup over classical computation? The answer is yes in the context of the some important applications. For example, when designing nonlinear optical systems in the pump depletion regime, one solves the three-wave problem to optimize the input seed pulse shape that is needed for achieving the desired output [31–33]. As another example, in the wave-kinetic approach to weak turbulence, one solves a network of wave-wave equations to determine the turbulence spectrum [34]. Finally, in inertial confinement fusion, laser beams exchange energy in plasma, and one solves the three-wave equations to compute the energy delivered to the fuel capsule [35]. In these applications, the inputs and outputs are simple, while each intermediate step involves  $D \times D$  matrices acting on an initial state  $\psi$ , where  $D$  is the number of wave states. On classical computers, computing  $U_N \dots U_2 U_1 \psi$  involves  $O(ND^2)$  operations, because even if  $U_j$  is sparse, the products may not be. In comparison, on quantum computers, assuming that cubic gates are prefabricated, then each step only involves the application of  $O(N)$  cubic gates. In this way, quantum computers may be used as special-purpose accelerators for these calculations.

In this letter, we demonstrate that effective cubic couplings can be realized without special-purpose hardware modifications and that precompiled three-wave gates can

be used in subsequent calculations. As a point example, consider laser-plasma interactions in the slowly-varying amplitude regime, which may be a subproblem of some more complex problems. After averaging over fast wave phases, the wave envelopes  $A_j$  of lasers and collective plasma excitations satisfy [26]

$$d_t A_1 = g A_2 A_3, \quad (2)$$

$$d_t A_2 = -g^* A_1 A_3^\dagger, \quad (3)$$

$$d_t A_3 = -g^* A_1 A_2^\dagger, \quad (4)$$

where  $d_t = \partial_t + \mathbf{v}_j \cdot \nabla$  is the convective derivative at the wave group velocity  $\mathbf{v}_j = \partial\omega_j/\partial\mathbf{k}_j$ , and the strength of the interaction is determined by the coupling coefficient  $g$ . The above equations are valid for resonant interactions, assuming that the positive wave frequencies satisfy  $\omega_1 = \omega_2 + \omega_3$  and the wave vectors satisfy  $\mathbf{k}_1 = \mathbf{k}_2 + \mathbf{k}_3$ . Near-resonant interactions may also be described by allowing a phase mismatch, which introduces a detuning term  $\exp(i\delta\mathbf{k} \cdot \mathbf{x} - i\delta\omega \cdot t)$  into the equations.

The above three-wave equations can be derived classically, in which  $A_j$  are complex numbers, as well as quantum mechanically, in which  $A_j$  are operators that satisfy commutation relations  $[A_j, A_l^\dagger] = \delta_{jl}$ . In the later case, consider the temporal problem where spatial derivatives vanish, then the three-wave equations become the Heisenberg equations, where the Hamiltonian is given by

$$H = ig A_1^\dagger A_2 A_3 - ig^* A_1 A_2^\dagger A_3^\dagger. \quad (5)$$

In the more general case where waves have spatial dependencies, the above procedure can be applied to each spatial Fourier component of the waves, thereby promoting a quantum mechanics problem to a quantum field theory problem [36]. Due to the limited number of qubits currently available, in what follows, we will only discuss the temporal problem, which can also be mapped to a steady-state problem in one spatial dimension.

To solve the three-wave problem on quantum computers, a naive approach is to map the wave envelope  $A_j$  to qubit  $a_j$ . However, this mapping has two major limitations. First, the qubit can only be in a superposition of  $|0\rangle$  and  $|1\rangle$  states, while a large amplitude wave, such as that of a laser, involves many photons. Therefore, representing the wave states requires a large number of qubits, and the naive mapping is inefficient. Second, the qubit frequency  $\Omega_j$  is not easily tunable [37] to match the three-wave resonance condition for  $\omega_j$ . Moreover, it is common that  $\omega_j \gg \omega_k$ , which makes it a stiff problem to emulate  $H$  using  $H_0$ , in which qubits usually have comparable frequencies.

Instead of mapping in the energy space, a more useful mapping can be attained in the action space. To see this, it is important to note that  $H$  does not contain generic cubic terms like  $A_1^\dagger A_2^\dagger A_3^\dagger$ . Due to the special form of  $H$ ,

the action operators

$$S_2 = n_1 + n_3, \quad (6)$$

$$S_3 = n_1 + n_2, \quad (7)$$

commute with the Hamiltonian, where  $n_j = A_j^\dagger A_j$  is the number operator. We can therefore look for simultaneous eigenstates of  $H$ ,  $S_2$ , and  $S_3$ . Denoting  $|0\rangle$  the vacuum state,  $|n_j\rangle = (A_j^\dagger)^{n_j}|0\rangle/\sqrt{n_j!}$  the  $n_j$ -th excited state of wave  $j$ , and  $|n_1, n_2, n_3\rangle = |n_1\rangle \otimes |n_2\rangle \otimes |n_3\rangle$ . Then, the simultaneous eigenspace of  $S_2$  and  $S_3$  has dimension  $D = \min(s_2, s_3) + 1$ , where the integer  $s_j \geq 0$  is the eigenvalue of  $S_j$ . Without loss of generality, suppose  $s_2 \leq s_3$ , which breaks the  $2 \leftrightarrow 3$  symmetry. Then, any state in the  $D$ -dimensional subspace  $V$  is spanned by

$$|\psi\rangle = \sum_{j=0}^{s_2} c_j |s_2 - j, s_3 - s_2 + j, j\rangle, \quad (8)$$

where the expansion coefficients satisfy the normalization condition  $\sum_j |c_j|^2 = 1$ . It is easy to check that  $S_2|\psi\rangle = s_2|\psi\rangle$  and  $S_3|\psi\rangle = s_3|\psi\rangle$ . Moreover, it is important to recognize that  $V$  is a closed subspace under the action of  $H$ , namely,  $H|\psi\rangle \in V$  whenever  $|\psi\rangle \in V$ . Therefore, the total Hilbert space of the three-wave system can be decomposed into a direct sum of invariant subspaces, and it is sufficient to solve the quantum problem within each subspace. Notice that using  $D = s_2 + 1$  levels, the above mapping can represent up to  $s_3$  photons. When  $s_3 \gg s_2$  the action-space mapping is much more efficient than the energy-space mapping.

Moreover, in the invariant subspace, the nonlinear three-wave problem becomes a linear quantum mechanical problem. The quantum problem can be solved in the Schrödinger picture, where  $i\partial_t|\psi\rangle = H|\psi\rangle$  becomes a system of equations for the time-dependent coefficient  $c_j(t)$ , which satisfies

$$i\partial_t c_j = ig h_{j+\frac{1}{2}} c_{j+1} - ig^* h_{j-\frac{1}{2}} c_{j-1}, \quad (9)$$

where  $h_{j-\frac{1}{2}} = \sqrt{j(s_2 + 1 - j)(s_3 - s_2 + j)}$  with  $h_{-\frac{1}{2}} = h_{D+\frac{1}{2}} = 0$ . Notice that  $H$  is now block tridiagonal with zero diagonal elements. In other words, frequencies  $\omega_j$  of the three-wave problem do not enter. This feature allows the use of qubits with a different set of frequencies  $\Omega_j$  to represent an arbitrary three-wave problems. Beyond pure states, dynamics of the full density matrix can be derived similarly.

Once the expansion coefficients are solved for given initial conditions, observables of interest can be evaluated by  $O(D)$  classical operations during post processing. For example, the occupation numbers of the three waves are given by  $\langle n_1 \rangle = \sum_{j=0}^{s_2} (s_2 - j) |c_j|^2$ ,  $\langle n_2 \rangle = \sum_{j=0}^{s_2} (s_3 - s_2 + j) |c_j|^2$ , and  $\langle n_3 \rangle = \sum_{j=0}^{s_2} j |c_j|^2$ . Higher-order cumulants, thereby all possible expectation values of interest, can be obtained similarly, and the three-wave problem is then solved. In other words, by mapping in

the action space, the nonlinear three-wave problem is reduced to a linear Hamiltonian simulation problem, whose goal is to determine the final states for given initial states.

To better understand the behavior of the quantum system, it is helpful to also analyze it using the Heisenberg picture. In particular, the number operators satisfy

$$\begin{aligned}\partial_t^2 n_1 &= -\partial_t^2 n_2 = -\partial_t^2 n_3 \\ &= 2|g|^2 [s_2 s_3 - (2s_2 + 2s_3 + 1)n_1 + 3n_1^2].\end{aligned}\quad (10)$$

In comparison, the classical wave actions  $I_j = |A_j|^2$ , where  $A_j$  are treated as complex numbers, satisfy

$$\begin{aligned}\partial_t^2 I_1 &= -\partial_t^2 I_2 = -\partial_t^2 I_3 \\ &= 2|g|^2 [s_2 s_3 - (2s_2 + 2s_3)I_1 + 3I_1^2].\end{aligned}\quad (11)$$

The quantum system may be used to approximate the classical system by identifying  $I_j \simeq \langle n_j \rangle$ . The error of such an identification is proportional to  $3(\langle n_1^2 \rangle - \langle n_1 \rangle^2) - \langle n_1 \rangle$ . The error terms in the parenthesis are small when the state is a well-localized semi-classical state, whose uncertainty is much smaller than its expectation value. The second error term is small when stimulated processes dominate spontaneous emission, which occurs when the wave amplitudes, or equivalently  $s_2$  and  $s_3$ , are large. When both contributions are small, the system is in the classical regime [38], and the solution given by the quantum system approaches the classical solution. On the other hand, when either contribution is large, the behaviors of the quantum and the classical systems are very different. For example, in the thermodynamic limit  $|c_j| = 1/D$ , the quantum system is stationary, whereas the classical three-wave system is not, which can be solved in terms of Jacobi elliptic functions [39, 40].

A nontrivial three-wave problem can already be solved using 3 levels, or equivalently, the  $|00\rangle$ ,  $|01\rangle$ , and  $|10\rangle$  states of two qubits. The allowable dimension is then  $D \leq 3$ . To utilize all levels, we can take  $s_2 = 2$  and  $s_3 = s \geq 2$ . In this case, a natural mapping is given by  $|2, s-2, 0\rangle = (1, 0, 0)^T$ ,  $|1, s-1, 1\rangle = (0, 1, 0)^T$ , and  $|0, s, 2\rangle = (0, 0, 1)^T$ . The normalized Hamiltonian matrix  $h = H/|g|$ , when restricted to the invariant subspace, is given by

$$h(\theta, s) = \begin{pmatrix} 0 & e^{i\theta} \sqrt{2(s-1)} & 0 \\ e^{-i\theta} \sqrt{2(s-1)} & 0 & e^{i\theta} \sqrt{2s} \\ 0 & e^{-i\theta} \sqrt{2s} & 0 \end{pmatrix}, \quad (12)$$

where  $\exp(i\theta) = ig/|g|$ . This time-independent Hamiltonian can be analytically exponentiated (Supplemental Material) to determine the unitary time-evolution operator  $U(\tau, \theta, s) = \exp[-ih(\theta, s)\tau]$ , where  $\tau = |g|\Delta t$  is the normalized time step. In the following, the goal is to realize three-wave gates  $U(\tau, \theta, s)$  on quantum computers. It is worth emphasizing that the three-level problem is a special example, and a general three-wave gate is associated with a  $D \times D$  unitary matrix. In other words,  $D$

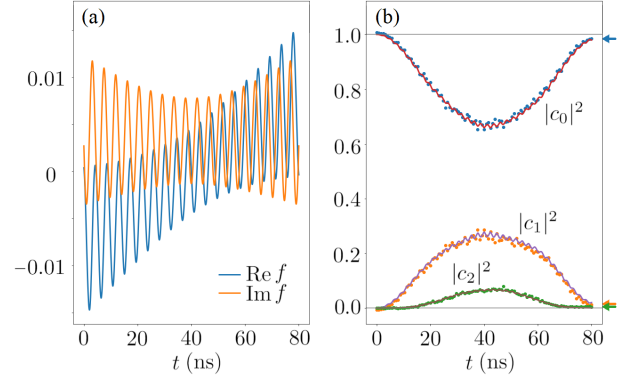


FIG. 1. (a) Optimized control pulse  $f(t)$  for achieving the unitary operator  $U(0.1, \pi/2, 2)$  on QuDIT. (b) Experimentally measured occupation numbers  $|c_n|^2$  (dots) during the control pulse application are well explained by solutions to the master equation (lines) when the qudit is initialized in the ground state. The agreement is comparable when the qudit is initialized in other states. At the end of the pulse application, the targeted transition probabilities (arrows) are attained.

needs not be three, but the Hamiltonian matrix is always tridiagonal, for which there exist efficient numerical algorithms to approximate its exponential [41]. The resultant unitary matrix is an input for the compilers.

The standard approach of compiling a unitary operator is using trotterization, whereby the operator is approximated by products of standard gates. As an example of state-of-the-art quantum cloud services, we implement the three-wave gate on Aspen-4-2Q-A of Rigetti Computing [42? ]. The probabilistic Quil compiler typically converts the three-wave gates to a sequence of  $\sim 20$  native gates, including two CZ gates for the three-level problem (Supplemental Material).

As an alternative approach, the unitary operator can also be compiled using control pulse engineering. Instead of preparing control pulses for standard gates and then using them to approximate customized gates, our approach directly prepare control pulses for customized gates. Our quantum hardware, QuDIT, is a dipole-enhanced Josephson-junction transmon qudit placed inside a three-dimensional superconducting microwave cavity, whose details are described in [43]. This architecture enhances the coherence time, while minimizing the number of control lines required to access larger computational spaces [44–49]. The control Hamiltonian is

$$H_c(t) \simeq \sum_j f_j(t) c_j^\dagger + f_j^*(t) c_j, \quad (13)$$

where  $f_j(t)$  is the complex-valued envelope of a microwave field whose carrier frequency is centered around  $\Omega_j$ , and  $c_j$  is the control operator (Supplemental Material). Since an arbitrary waveform can be generated by

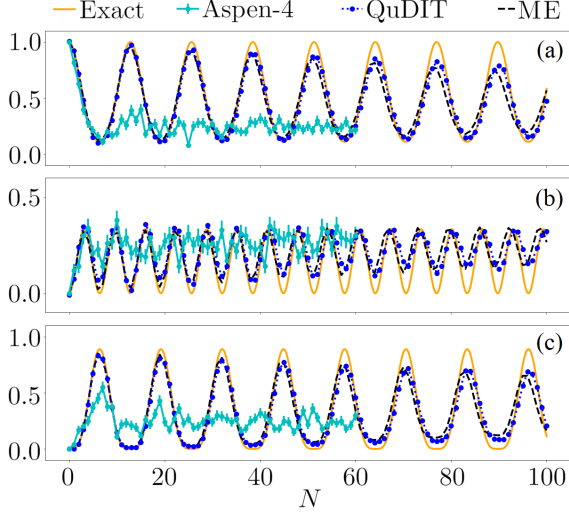


FIG. 2. Occupation probabilities of (a)  $|0\rangle$ , (b)  $|1\rangle$ , and (c)  $|2\rangle$  states after  $N$  repetitions of the three-wave gate  $U(0.2, \pi/2, 2)$  when the quantum computer is initialized in the ground state. On Aspen-4 (cyan), the three-wave gate is realized using  $\sim 20$  native gates, and the allowable repetition is limited to  $N \sim 10$ , before the results deviate unacceptably from the exact solutions (orange). On QuDIT (blue), the three-wave gate is realized by a single control pulse, and the allowable repetition is extended to  $N \sim 100$ , whose results are well explained by solutions of the Lindblad master equation (black).

digital synthesis, the control is universal [50, 51] and the time dependence of  $f_j(t)$  can be engineered such that

$$\mathcal{T}e^{-i\int_0^T dt[H_0+H_c(t)]} \simeq e^{-iH\Delta t}, \quad (14)$$

where  $\mathcal{T}$  is the time-ordering operator,  $T$  is the length of the control pulse, and  $\Delta t$  is the time step size. The control waveform is not unique, but may be designed using numerical optimization, for example, with the gradient ascent pulse engineering algorithm [52].

As a test problem, we construct a control pulse to achieve  $U(\tau, \theta, s)$  for  $\tau = 0.1$ ,  $\theta = \pi/2$ , and  $s = 2$ . The control pulse is generated using the built-in function `optimize_pulse_unitary` in QuTIP [53, 54], neglecting noise processes. The optimization is started with zero as the initial guess, and is constrained to have a maximum drive strength  $|f| < 0.03$  in normalized units. Two forbidden levels beyond the  $D = 3$  levels are included in the optimization to suppress possible state leakage. The control pulse is designed to have a duration of  $T = 80$  ns. This pulse duration is much shorter than the coherence time but long enough to allow the lowest three levels of our qudit, which has an anharmonicity of  $\sim 0.2$  GHz, to be separately addressed. The real and imaginary parts of the optimized pulse envelope are shown in Fig. 1(a), which are obtained after  $\sim 10$  optimization iterations. The optimization takes a few seconds on a single-core computer, and further iterations do not significantly improve the

fidelity, whose error target is set to be  $10^{-5}$ . The optimized wave form is then mixed with a carrier frequency centered at the qudit  $|0\rangle \leftrightarrow |1\rangle$  transition at 4.1 GHz, and is synthesized digitally using a Keysight 8195A arbitrary waveform generator with a 32-GHz sampling rate. The occupation of the three levels are measured using dispersive readout [44] with a traveling wave parametric amplifier [55, 56] followed by a ZVA-183W-S+ amplifier. Readout errors are partially corrected using a confusion matrix [43]. The occupations during the pulse application are shown in Fig. 1(b), when the qudit is initialized in the ground state. The experimentally measured results (dots) are well explained by numerical solutions (lines) of the Lindblad master equation [57–61], when hardware-specific decay and dephasing are taken into account (Supplemental Material). At the end of the control pulse, the intended unitary operator is realized, and the targeted transition probabilities (arrows) are attained.

Using either approach, we can now repeatedly apply the prefabricated three-wave gates to compute the temporal three-wave problem. With the quantum computer initialized in the ground state, we read out the occupation probabilities after  $N$  gate applications, and compare the results with the exact solutions (Fig. 2, orange). Using customized control pulses, the experimental results on QuDIT (blue) follow the exact solutions closely up to  $N \sim 100$ , and the deviations can be explained by the master equation solutions (black) using our noise model (Supplemental Material). In comparison, using trotterization, the experimental results on Aspen-4 (cyan) track the exact results up to  $N \sim 10$ . However, it is worth emphasizing that the hardware performance of both quantum computers is comparable. The differences are mainly due to the fact that the trotterization approach requires  $\sim 20$  gates while the customized-control approach only requires a single gate for each computational step. In other words, both quantum computers can perform  $\sim 100$  gates with high fidelity, and the better results on QuDIT can mostly be attributed to the control pulse engineering approach instead of the hardware differences.

In addition to reducing the gate depth, the customized-control approach may also alleviate the compilation overhead of parametric gates when interpolation is employed. Using the interpolation as a shortcut is not guaranteed to work, but can expedite calculations in more complex problems where gates at a variety of parameter values are needed. For example, consider a one-parameter family of three-wave gates  $U(s)$ , which can be costly to compile on classical computers. Fortunately, it turns out that we can precompile the gates at two  $s$  values, and the interpolated control pulse at intermediate  $s$  is capable of driving high-fidelity results. Our interpolation scheme is based on the observation that  $h(s) = \sqrt{2}s[(1-\xi)K(2) + (\xi - 1/\sqrt{2})K(\infty)]/(1 - 1/\sqrt{2})$ , where  $\xi(s) = \sqrt{1 - 1/s}$ , and the nonzero elements of

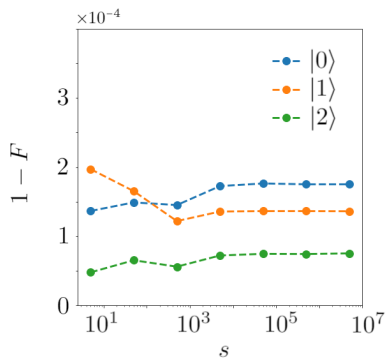


FIG. 3. Interpolated control pulses are able to drive high-fidelity quantum computations for a wide range of  $s$  parameters when the qudit is initialized in  $|0\rangle$  (blue),  $|1\rangle$  (orange), and  $|2\rangle$  (green) states. The interpolation only uses optimized control pulses at  $s = 2$  and  $s = \infty$ , for fixed  $\tau\sqrt{2s} = 0.2$  and  $\theta = \pi/2$ . The single-gate fidelity is numerically obtained from solutions of the master equation, by comparing the density matrices result from interpolated versus optimized pulses.

the symmetric  $3 \times 3$  matrix  $K$  are  $K_{12}(s) = \xi$  and  $K_{23}(s) = 1$ . Motivated by this form, the interpolated control pulse for  $s \geq 2$  at each time slice is taken to be  $\epsilon_I(s) = [(1 - \xi)\epsilon_O(2) + (\xi - 1/\sqrt{2})\epsilon_O(\infty)]/(1 - 1/\sqrt{2})$ , where  $\epsilon_O(s)$  denotes the optimized pulse, and  $\tau\sqrt{2s} = 0.2$  is held a constant. In other words, we interpolate the control pulse using the same formula for interpolating the Hamiltonian. Although this scheme is not proven to work in general, for the three-level problem, the interpolated pulses are able to achieve comparable high fidelity as the optimized pulses when used to drive the quantum computation (Fig. 3). The fidelity is obtained by numerically solving the master equation, and is defined by  $F(\rho, \sigma) = \text{tr}\sqrt{\rho^{1/2}\sigma\rho^{1/2}}$  [7], where  $\rho$  and  $\sigma$  are the density matrices attained using optimized and interpolated pulses after one gate application.

In summary, we demonstrate that cubic couplings, which are absent from the quantum hardware, can be generated effectively by mapping in the action space. The resultant three-wave gates are basic building blocks in many nonlinear physics problems, whose simulations may harness quantum speedup when precompiled gates are employed. Using three levels as a minimum nontrivial example, we verify that the compilation can be achieved on quantum cloud services using trotterization, which requires a large number of native gates and is therefore severely restricted by decoherence on noisy quantum computers. As a more efficient approach, we compile the targeted cubic coupling as a single three-wave gate using an optimized control pulse, thereby saving the precious quantum resources for the end application. Applying customized pulses on QuDIT, high-fidelity results are obtained for the temporal three-wave problem, and ten times more computational steps can now be carried out.

In addition, reliable control pulses may also be generated by interpolation, which reduces the compilation cost of parametric gates. With more available qubits and longer coherence time in the future, these quantum cubic gates may be used to compute interesting problems in nonlinear optics, weak turbulence, and lattice gauge theories.

We would like to thank Rigetti Computing for providing access to their 16Q Aspen-4 processor, where we used lattice Aspen-4-2Q-A. Y. S. would like to thank Eric T. Holland, Xian Wu, and Hong Qin for helpful discussions. This work was performed under the auspices of US Department of Energy (DOE) by LLNL under Contract DE-AC52-07NA27344. The experimental work was supported by the DOE Office of Fusion Energy Sciences “Quantum Leap for Fusion Energy Sciences” under project FWP-SCW1680, and the theory work was supported by LLNL-LDRD under Project 19-FS-072. The QuDIT was funded under the National Nuclear Security Administration (NNSA) Advanced Simulation and Computing (ASC) “Beyond Moore’s Law” quantum program under NA-ASC-127R-16 and US DOE, Office of Science, Office of Advanced Scientific Computing Research, Quantum Testbed Pathfinder Program under Award 2017-LLNL-SCW1631. Y. S. was supported by the Lawrence Fellowship through LLNL-LDRD under Project 19-ERD-038.

---

\* shi9@llnl.gov

- [1] A. Barenco, C. H. Bennett, R. Cleve, D. P. DiVincenzo, N. Margolus, P. Shor, T. Sleator, J. A. Smolin, and H. Weinfurter, Elementary gates for quantum computation, *Phys. Rev. A* **52**, 3457 (1995).
- [2] B. P. Lanyon, C. Hempel, D. Nigg, M. Müller, R. Geritsma, F. Zähringer, P. Schindler, J. T. Barreiro, M. Rambach, G. Kirchmair, M. Hennrich, P. Zoller, R. Blatt, and C. F. Roos, Universal digital quantum simulation with trapped ions, *Science* **334**, 57 (2011).
- [3] M. Mariantoni, H. Wang, T. Yamamoto, M. Neeley, R. C. Bialczak, Y. Chen, M. Lenander, E. Lucero, A. D. O’Connell, D. Sank, M. Weides, J. Wenner, Y. Yin, J. Zhao, A. N. Korotkov, A. N. Cleland, and J. M. Martinis, Implementing the quantum von neumann architecture with superconducting circuits, *Science* **334**, 61 (2011).
- [4] U. L. Heras, A. Mezzacapo, L. Lamata, S. Filipp, A. Wallraff, and E. Solano, Digital quantum simulation of spin systems in superconducting circuits, *Phys. Rev. Lett.* **112**, 200501 (2014).
- [5] A. Mezzacapo, U. Las Heras, J. Pedernales, L. DiCarlo, E. Solano, and L. Lamata, Digital quantum rabi and dicke models in superconducting circuits, *Sci. Rep.* **4**, 7482 (2014).
- [6] Y. Salathé, M. Mondal, M. Oppliger, J. Heinsoo, P. Kurpiers, A. Potočnik, A. Mezzacapo, U. Las Heras, L. Lamata, E. Solano, S. Filipp, and A. Wallraff, Digital quantum simulation of spin models with circuit quantum electrodynamics, *Phys. Rev. X* **5**, 021027 (2015).



- [7] M. A. Nielsen and I. Chuang, *Quantum computation and quantum information* (Cambridge University Press, 2010).
- [8] N. Ofek, A. Petrenko, R. Heeres, P. Reinhold, Z. Leghtas, B. Vlastakis, Y. Liu, L. Frunzio, S. Girvin, L. Jiang, *et al.*, Extending the lifetime of a quantum bit with error correction in superconducting circuits, *Nature* **536**, 441 (2016).
- [9] F. Reiter, A. S. Sørensen, P. Zoller, and C. Muschik, Dissipative quantum error correction and application to quantum sensing with trapped ions, *Nat. Commun.* **8**, 1822 (2017).
- [10] S. Rosenblum, P. Reinhold, M. Mirrahimi, L. Jiang, L. Frunzio, and R. J. Schoelkopf, Fault-tolerant detection of a quantum error, *Science* **361**, 266 (2018).
- [11] S. Rosenblum, Y. Y. Gao, P. Reinhold, C. Wang, C. J. Axline, L. Frunzio, S. M. Girvin, L. Jiang, M. Mirrahimi, M. H. Devoret, *et al.*, A CNOT gate between multiphoton qubits encoded in two cavities, *Nat. Commun.* **9**, 652 (2018).
- [12] R. Gerritsma, G. Kirchmair, F. Zähringer, E. Solano, R. Blatt, and C. F. Roos, Quantum simulation of the Dirac equation, *Nature* **463**, 68 (2010).
- [13] Y. Chen, P. Roushan, D. Sank, C. Neill, E. Lucero, M. Mariantoni, R. Barends, B. Chiaro, J. Kelly, A. Megrant, *et al.*, Emulating weak localization using a solid-state quantum circuit, *Nat. Commun.* **5**, 5184 (2014).
- [14] P. Roushan, C. Neill, Y. Chen, M. Kolodrubetz, C. Quintana, N. Leung, M. Fang, R. Barends, B. Campbell, Z. Chen, *et al.*, Observation of topological transitions in interacting quantum circuits, *Nature* **515**, 241 (2014).
- [15] J. Braumüller, M. Marthaler, A. Schneider, A. Stehli, H. Rotzinger, M. Weides, and A. V. Ustinov, Analog quantum simulation of the Rabi model in the ultra-strong coupling regime, *Nat. Commun.* **8**, 779 (2017).
- [16] P. Roushan, C. Neill, J. Tangpanitanon, V. M. Bastidas, A. Megrant, R. Barends, Y. Chen, Z. Chen, B. Chiaro, A. Dunsworth, A. Fowler, B. Foxen, M. Giustina, E. Jeffrey, J. Kelly, E. Lucero, J. Mutus, M. Neeley, C. Quintana, D. Sank, A. Vainsencher, J. Wenner, T. White, H. Neven, D. G. Angelakis, and J. Martinis, Spectroscopic signatures of localization with interacting photons in superconducting qubits, *Science* **358**, 1175 (2017).
- [17] P. Roushan, C. Neill, A. Megrant, Y. Chen, R. Babush, R. Barends, B. Campbell, Z. Chen, B. Chiaro, A. Dunsworth, *et al.*, Chiral ground-state currents of interacting photons in a synthetic magnetic field, *Nat. Phys.* **13**, 146 (2017).
- [18] N. Langford, R. Sagastizabal, M. Kounalakis, C. Dickel, A. Bruno, F. Luthi, D. Thoen, A. Endo, and L. DiCarlo, Experimentally simulating the dynamics of quantum light and matter at deep-strong coupling, *Nat. Commun.* **8**, 1715 (2017).
- [19] A. Kandala, A. Mezzacapo, K. Temme, M. Takita, M. Brink, J. M. Chow, and J. M. Gambetta, Hardware-efficient variational quantum eigensolver for small molecules and quantum magnets, *Nature* **549**, 242 (2017).
- [20] C. Neill, P. Roushan, K. Kechedzhi, S. Boixo, S. V. Isakov, V. Smelyanskiy, A. Megrant, B. Chiaro, A. Dunsworth, K. Arya, R. Barends, B. Burkett, Y. Chen, Z. Chen, A. Fowler, B. Foxen, M. Giustina, R. Graff, E. Jeffrey, T. Huang, J. Kelly, P. Klimov, E. Lucero, J. Mutus, M. Neeley, C. Quintana, D. Sank, A. Vainsencher, J. Wenner, T. C. White, H. Neven, and J. M. Martinis, A blueprint for demonstrating quantum supremacy with superconducting qubits, *Science* **360**, 195 (2018).
- [21] R. Harris, Y. Sato, A. J. Berkley, M. Reis, F. Altomare, M. H. Amin, K. Boothby, P. Bunyk, C. Deng, C. Enderud, S. Huang, E. Hoskinson, M. W. Johnson, E. Ladizinsky, N. Ladizinsky, T. Lanting, R. Li, T. Medina, R. Molavi, R. Neufeld, T. Oh, I. Pavlov, I. Perminov, G. Poulin-Lamarre, C. Rich, A. Smirnov, L. Swenson, N. Tsai, M. Volkmann, J. Whittaker, and J. Yao, Phase transitions in a programmable quantum spin glass simulator, *Science* **361**, 162 (2018).
- [22] E. T. Holland, K. A. Wendt, K. Kravvaris, X. Wu, W. E. Ormand, J. Dubois, S. Quaglion, and F. Pederiva, Quantum hardware aware encoding for the real-time dynamics of a neutron-neutron interaction, *arXiv* (2019).
- [23] C.-N. Yang and R. L. Mills, Conservation of isotopic spin and isotopic gauge invariance, *Phys. Rev.* **96**, 191 (1954).
- [24] N. Bloembergen, *Nonlinear Optics* (World Scientific, 1996).
- [25] V. E. Zakharov, V. L'vov, and G. Falkovich, *Kolmogorov spectra of turbulence* (Springer-Verlag, 1992).
- [26] R. Davidson, *Methods in Nonlinear Plasma Theory* (Academic Press, 1972).
- [27] H. Häffner, C. F. Roos, and R. Blatt, Quantum computing with trapped ions, *Phys. Rep.* **469**, 155 (2008).
- [28] J. Clarke and F. K. Wilhelm, Superconducting quantum bits, *Nature* **453**, 1031 (2008).
- [29] J. M. Chow, L. DiCarlo, J. M. Gambetta, F. Motzoi, L. Frunzio, S. M. Girvin, and R. J. Schoelkopf, Optimized driving of superconducting artificial atoms for improved single-qubit gates, *Phys. Rev. A* **82**, 040305 (2010).
- [30] S. E. Nigg, H. Paik, B. Vlastakis, G. Kirchmair, S. Shankar, L. Frunzio, M. H. Devoret, R. J. Schoelkopf, and S. M. Girvin, Black-box superconducting circuit quantization, *Phys. Rev. Lett.* **108**, 240502 (2012).
- [31] L. M. Frantz and J. S. Nodvik, Theory of pulse propagation in a laser amplifier, *J. Appl. Phys.* **34**, 2346 (1963).
- [32] J. Ahn, A. Efimov, R. Averitt, and A. Taylor, Terahertz waveform synthesis via optical rectification of shaped ultrafast laser pulses, *Opt. Express* **11**, 2486 (2003).
- [33] G. Brunton, G. Erbert, D. Browning, and E. Tse, The shaping of a national ignition campaign pulsed waveform, *Fusion Eng. Des.* **87**, 1940 (2012).
- [34] V. E. Zakharov, V. S. L'vov, and G. Falkovich, *Kolmogorov spectra of turbulence I: Wave turbulence* (Springer Science & Business Media, 2012).
- [35] J. F. Myatt, J. Zhang, R. W. Short, A. V. Maximov, W. Seka, D. H. Froula, D. H. Edgell, D. T. Michel, I. V. Igumenshchev, D. E. Hinkel, *et al.*, Multiple-beam laser-plasma interactions in inertial confinement fusion, *Phys. Plasmas* **21**, 055501 (2014).
- [36] Y. Shi, H. Qin, and N. J. Fisch, Three-wave scattering in magnetized plasmas: From cold fluid to quantized Lagrangian, *Phys. Rev. E* **96**, 023204 (2017).
- [37] Y. Chen, C. Neill, P. Roushan, N. Leung, M. Fang, R. Barends, J. Kelly, B. Campbell, Z. Chen, B. Chiaro, A. Dunsworth, E. Jeffrey, A. Megrant, J. Y. Mutus, P. J. J. O'Malley, C. M. Quintana, D. Sank, A. Vainsencher, J. Wenner, T. C. White, M. R. Geller, A. N. Cleland, and J. M. Martinis, Qubit architecture with high coherence and fast tunable coupling, *Phys.*

- Rev. Lett. **113**, 220502 (2014).
- [38] E. T. Jaynes and F. W. Cummings, Comparison of quantum and semiclassical radiation theories with application to the beam maser, *Proc. IEEE* **51**, 89 (1963).
  - [39] A. Jurkus and P. Robson, Saturation effects in a travelling-wave parametric amplifier, *Proceedings of the IEE-Part B: Electronic and Communication Engineering* **107**, 119 (1960).
  - [40] J. A. Armstrong, N. Bloembergen, J. Ducuing, and P. S. Pershan, Interactions between light waves in a nonlinear dielectric, *Phys. Rev.* **127**, 1918 (1962).
  - [41] F. R. Graziani, The product formula algorithm applied to linear and radiation diffusion, *J. Comp. Phys.* **118**, 9 (1995).
  - [42] R. S. Smith, M. J. Curtis, and W. J. Zeng, A practical quantum instruction set architecture, *arXiv:1608.03355* (2016).
  - [43] X. Wu *et al.*, Full characterization and universal control of a transmon qudit, to be published (2020).
  - [44] A. Blais, R.-S. Huang, A. Wallraff, S. M. Girvin, and R. J. Schoelkopf, Cavity quantum electrodynamics for superconducting electrical circuits: An architecture for quantum computation, *Phys. Rev. A* **69**, 062320 (2004).
  - [45] A. Wallraff, D. I. Schuster, A. Blais, L. Frunzio, R.-S. Huang, J. Majer, S. Kumar, S. M. Girvin, and R. J. Schoelkopf, Strong coupling of a single photon to a superconducting qubit using circuit quantum electrodynamics, *Nature* **431**, 162 (2004).
  - [46] J. Koch, T. M. Yu, J. Gambetta, A. A. Houck, D. I. Schuster, J. Majer, A. Blais, M. H. Devoret, S. M. Girvin, and R. J. Schoelkopf, Charge-insensitive qubit design derived from the Cooper pair box, *Phys. Rev. A* **76**, 042319 (2007).
  - [47] J. A. Schreier, A. A. Houck, J. Koch, D. I. Schuster, B. R. Johnson, J. M. Chow, J. M. Gambetta, J. Majer, L. Frunzio, M. H. Devoret, S. M. Girvin, and R. J. Schoelkopf, Suppressing charge noise decoherence in superconducting charge qubits, *Phys. Rev. B* **77**, 180502 (2008).
  - [48] H. Paik, D. I. Schuster, L. S. Bishop, G. Kirchmair, G. Catelani, A. P. Sears, B. R. Johnson, M. J. Reagor, L. Frunzio, L. I. Glazman, S. M. Girvin, M. H. Devoret, and R. J. Schoelkopf, Observation of high coherence in josephson junction qubits measured in a three-dimensional circuit QED architecture, *Phys. Rev. Lett.* **107**, 240501 (2011).
  - [49] C. Rigetti, J. M. Gambetta, S. Poletto, B. L. T. Plourde, J. M. Chow, A. D. Córcoles, J. A. Smolin, S. T. Merkel, J. R. Rozen, G. A. Keefe, M. B. Rothwell, M. B. Ketchen, and M. Steffen, Superconducting qubit in a waveguide cavity with a coherence time approaching 0.1 ms, *Phys. Rev. B* **86**, 100506 (2012).
  - [50] J. Raftery, A. Vrajitoarea, G. Zhang, Z. Leng, S. Srinivasan, and A. Houck, Direct digital synthesis of microwave waveforms for quantum computing, *arXiv:1703.00942* (2017).
  - [51] R. W. Heeres, P. Reinhold, N. Ofek, L. Frunzio, L. Jiang, M. H. Devoret, and R. J. Schoelkopf, Implementing a universal gate set on a logical qubit encoded in an oscillator, *Nat. Commun.* **8**, 94 (2017).
  - [52] N. Khaneja, T. Reiss, C. Kehlet, T. Schulte-Herbrüggen, and S. J. Glaser, Optimal control of coupled spin dynamics: design of nmr pulse sequences by gradient ascent algorithms, *J. Magn. Reson.* **172**, 296 (2005).
  - [53] J. Johansson, P. Nation, and F. Nori, Qutip 2: A python framework for the dynamics of open quantum systems, *Comput. Phys. Commun.* **184**, 1234 (2013).
  - [54] J. R. Johansson, P. Nation, and F. Nori, Qutip: An open-source python framework for the dynamics of open quantum systems, *Comp. Phys. Commun.* **183**, 1760 (2012).
  - [55] K. O'Brien, C. Macklin, I. Siddiqi, and X. Zhang, Resonant phase matching of josephson junction traveling wave parametric amplifiers, *Phys. Rev. Lett.* **113**, 157001 (2014).
  - [56] C. Macklin, K. O'Brien, D. Hover, M. E. Schwartz, V. Bolkhovskiy, X. Zhang, W. D. Oliver, and I. Siddiqi, A near-quantum-limited Josephson traveling-wave parametric amplifier, *Science* **350**, 307 (2015).
  - [57] K. W. Murch, U. Vool, D. Zhou, S. J. Weber, S. M. Girvin, and I. Siddiqi, Cavity-assisted quantum bath engineering, *Phys. Rev. Lett.* **109**, 183602 (2012).
  - [58] K. Geerlings, Z. Leghtas, I. M. Pop, S. Shankar, L. Frunzio, R. J. Schoelkopf, M. Mirrahimi, and M. H. Devoret, Demonstrating a driven reset protocol for a superconducting qubit, *Phys. Rev. Lett.* **110**, 120501 (2013).
  - [59] Z. Leghtas, U. Vool, S. Shankar, M. Hatridge, S. M. Girvin, M. H. Devoret, and M. Mirrahimi, Stabilizing a bell state of two superconducting qubits by dissipation engineering, *Phys. Rev. A* **88**, 023849 (2013).
  - [60] E. T. Holland, B. Vlastakis, R. W. Heeres, M. J. Reagor, U. Vool, Z. Leghtas, L. Frunzio, G. Kirchmair, M. H. Devoret, M. Mirrahimi, and R. J. Schoelkopf, Single-photon-resolved cross-kerr interaction for autonomous stabilization of photon-number states, *Phys. Rev. Lett.* **115**, 180501 (2015).
  - [61] Z. Leghtas, S. Touzard, I. M. Pop, A. Kou, B. Vlastakis, A. Petrenko, K. M. Sliwa, A. Narla, S. Shankar, M. J. Hatridge, *et al.*, Confining the state of light to a quantum manifold by engineered two-photon loss, *Science* **347**, 853 (2015).
  - [62] Rigetti QCS is continuously upgraded and routinely calibrated. For data reported in this paper, the QCS was accessed on January 7th, 2020 at 12:30 PM.

### Unitary evolution of three levels

For the three-level problem, the Hamiltonian matrix [Eq. (12)] can be exponentiated analytically. The Schrödinger time evolution of the three levels is determined by the unitary matrix  $U = \exp(-ih\tau)$ , which is given explicitly by

$$U(\tau, \theta, s) = \begin{pmatrix} \frac{(s-1)\cos\lambda\tau+s}{2s-1} & -ie^{i\theta}\sqrt{\frac{s-1}{2s-1}}\sin\lambda\tau & e^{2i\theta}\frac{\sqrt{s(s-1)}}{2s-1}(\cos\lambda\tau-1) \\ -ie^{-i\theta}\sqrt{\frac{s-1}{2s-1}}\sin\lambda\tau & \cos\lambda\tau & -ie^{i\theta}\sqrt{\frac{s}{2s-1}}\sin\lambda\tau \\ e^{-2i\theta}\frac{\sqrt{s(s-1)}}{2s-1}(\cos\lambda\tau-1) & -ie^{-i\theta}\sqrt{\frac{s}{2s-1}}\sin\lambda\tau & \frac{s\cos\lambda\tau+s-1}{2s-1} \end{pmatrix}, \quad (\text{S.1})$$

where  $\lambda = \sqrt{2(2s-1)}$  is the positive eigenvalue of the Hamiltonian. The above  $3 \times 3$  unitary matrix can be embedded into a two-qubits system by acting it on the  $|00\rangle$ ,  $|01\rangle$ , and  $|10\rangle$  states, while leaving the  $|11\rangle$  state invariant.

The above unitary matrix is an input for both the trotterization and the customized-control approaches. For larger problems, the three-wave Hamiltonian remains tridiagonal, for which there exist efficient numerical algorithms to approximate its exponential [41]. Although it may seem that once the unitary matrix is known, the problem would have already been solved, it is worth noting that the three-wave gate may be a subproblem of some more complex problems. For example, in radiation hydrodynamics, lasers couple via three-wave interactions for given plasma conditions, while the plasma conditions evolve due to laser energy deposition. The self consistent equations may be solved using splitting algorithms, whose solutions may be written schematically as  $U_N V_N \dots U_1 V_1 U_0 V_0$ , where  $U$ 's are three-wave gates and  $V$ 's are gates that advance the plasma conditions. In problems of this type, knowing  $U$  is an intermediate step towards solving the entire problem, and quantum computing may be used to effectively carry out the matrix multiplications by applying prefabricated gates.

### Realizing three-wave gates on Rigetti QCS

As an example of state-of-the-art quantum cloud services (QCS), Rigetti Computing [?] offers a native gate set consists of single-qubit rotations  $R_x(\theta)$ ,  $R_z(\theta)$ , and two-qubit CZ gates. The Quil compiler uses these gates to approximate other unitary operators using non-deterministic algorithms [42], which efficiently generate approximations for a given error tolerance. In particular, the three-level unitary matrix  $U(\tau, \theta, s)$  can be declared as user-defined gate via the `DEFGATE` directive in the pyQuil library [42]. After routing to two adjacent qubits on the quantum hardware, the probabilistic compiler typically converts this three-wave gate to a sequence of  $\sim 20$  native gates, including two CZ gates (Fig. S1). When directly repeating the gate in pyQuil, the compiler multiplies  $U(\tau)^N = U(N\tau)$  and compiles for  $U(N\tau)$  instead. This default simplification, which offloads the burden of computation to classical computers, is suppressed by placing the gate sequence for  $U(\tau)$  within `PRAGMA PRESERVE_BLOCK` and `PRAGMA END_PRESERVE_BLOCK`. In this way,  $U(\tau)^N$  is realized on Rigetti's Aspen-4-2Q-A by applying precompiled  $U(\tau)$  for  $N$  times [62].

### Noise modeling using Lindblad master equation

Realistic quantum computers are open systems, and coupling to the environment is inevitable during control and readout operations. The state of a quantum computer, which is mixed with the environment, may be characterized by its density matrix. Assuming processes in the environment are stationary and Markovian, then time evolution of the density matrix may be described by the Lindblad master equation [57–61]

$$\partial_t \rho = i[\rho, H_0 + H_c(t)] + \sum_j (L_j \rho L_j^\dagger - \frac{1}{2}\{L_j^\dagger L_j, \rho\}), \quad (\text{S.2})$$

where we have used the unit  $\hbar = 1$ . The first term is the unitary evolution due to the bare Hamiltonian  $H_0$  of the quantum hardware, as well as the control Hamiltonian  $H_c(t)$  due to the application of the control pulse. In the second term, Lindblad operators  $L_j$  are used to model dissipative processes due to couplings with the environment. The above Lindblad master equation can be solved numerically using the built-in function `mesolve` in QuTIP [53, 54], once the Hamiltonians and the Lindbladians are specified.

To model the Quantum Design and Integration Testbed (QuDIT), the following Hamiltonians and the Lindbladians are used, whose parameters are measured experimentally [43] for the lowest three levels of the qudit, and then



extrapolated to higher levels. First, the transition frequencies and the effective drive Hamiltonian are measured using Rabi spectroscopy, and the combined dynamics generator for the quantum computer is  $H_0 + f(t)c + f^*(t)c^\dagger$ . Keeping the lowest five levels, we approximate

$$H_0 \simeq \begin{pmatrix} 0 & 0 & 0 & 0 & 0 \\ 0 & 25.758 & 0 & 0 & 0 \\ 0 & 0 & 50.099 & 0 & 0 \\ 0 & 0 & 0 & 72.848 & 0 \\ 0 & 0 & 0 & 0 & 93.828 \end{pmatrix}, \quad c \simeq \begin{pmatrix} 0 & 1.000 & 0 & 0 & 0 \\ 0 & 0 & -1.372 & 0 & 0 \\ 0 & 0 & 0 & -1.618 & 0 \\ 0 & 0 & 0 & 0 & 1.781 \\ 0 & 0 & 0 & 0 & 0 \end{pmatrix}, \quad (\text{S.3})$$

where angular frequencies are in units of  $2\pi$  GHz. Second, two Lindbladians are included to model decay and dephasing. The Lindblad operator  $L_1 \sim a$  describes successive decays to lower levels, whose nonzero matrix elements are  $L_1(j, j+1) = 1/\sqrt{T_1(j+1, j)}$ . The Lindblad operator  $L_2 \sim a^\dagger a$  describes dephasing with respect to lower levels, whose nonzero matrix elements are  $L_2(j, j) = 1/\sqrt{T_2^*(j, j-1)}$ . The  $T_1$  decay time and the  $T_2^*$  dephasing time, in units of ns, are measured using Ramsey spectroscopy between the  $j$ -th and the  $(j+1)$ -th levels, assuming the occupation probability of the  $j$ -th level can be fitted by  $A \exp[-t/T_2^*(j+1, j)] \cos(\omega t + \phi) + B \exp[-t/T_1(j, j-1)]$ . Keeping the lowest five levels, we approximate

$$L_1 \simeq \begin{pmatrix} 0 & 0.004 & 0 & 0 & 0 \\ 0 & 0 & 0.006 & 0 & 0 \\ 0 & 0 & 0 & 0.007 & 0 \\ 0 & 0 & 0 & 0 & 0.009 \\ 0 & 0 & 0 & 0 & 0 \end{pmatrix}, \quad L_2 \simeq \begin{pmatrix} 0 & 0 & 0 & 0 & 0 \\ 0 & 0.005 & 0 & 0 & 0 \\ 0 & 0 & 0.014 & 0 & 0 \\ 0 & 0 & 0 & 0.045 & 0 \\ 0 & 0 & 0 & 0 & 0.000 \end{pmatrix}. \quad (\text{S.4})$$

Parameters in the Hamiltonians and the Lindbladians may drift over time and change after each cool down. The above parameters are obtained from the QuDIT calibration immediately before the experimental runs that produce the data reported in the main text.

```

PRAGMA PRESERVE_BLOCK
PRAGMA INITIAL_REWIRING "GREEDY"
1  RZ(pi) 1
2  RX(1.570796326794897) 1
3  RZ(-0.955316618124509) 1
4  RX(1.5707963267948948) 2
5  CZ 1 2
6  RX(pi/2) 1
7  RZ(0.4898979485566355) 1
8  RX(-pi/2) 1
9  RZ(1.4274665982948886) 2
10 RX(pi/2) 2
11 RZ(0.3986464309139781) 2
12 RX(-pi/2) 2
13 CZ 1 2
14 RZ(-2.1862760354652844) 1
15 RX(pi/2) 1
16 RZ(-1.7141260552949014) 2
17 RX(-1.5707963267948963) 2
PRAGMA END_PRESERVE_BLOCK

:
DECLARE ro BIT[2]
MEASURE 0 ro[0]
MEASURE 1 ro[1]

```

}  $U(0.2, \pi/2, 2)$

FIG. S1. An example Quil program that implement a three-wave gate on Rigetti's Aspen-4. In this example,  $U(0.2, \pi/2, 2)$  is approximated by 17 native gates. This gate sequence can be repeated  $N$  times to realize  $U^N$  before the final readout.